The 2021 South Sandwich Island Mw 8.2 earthquake: a slow event sandwiched between regular ruptures

Zhe Jia[1], Zhongwen Zhan[1], and Hiroo Kanamori[1]

[1]California Institute of Technology

November 22, 2022

Abstract

We determined the rupture sequence of the Aug 12, 2021 Mw 8.2 South Sandwich Island earthquake which, according to the reports from the National Earthquake Information Center, appears to be a complex sequence in both time and space. Notable tsunamis were recorded by tide gauges at global distances. Given the complexity of this event, we used a multiple subevent inversion method that can accommodate complex variations of fault geometry, location, depth, and temporal characteristics of the event. We found that the rupture initiated as a regular deep thrust earthquake; it then triggered a shallow dominantly slow subevent extending ˜200 km to the south, and ended with 2 other regular subevents. The total duration is ˜260s, unusually long for an Mw 8.2 event. Our result is qualitatively consistent with other moment tensor solutions and the observed mB-Mw and MS-Mw relations, and provides a more quantitative space-temporal pattern of this unusual sequence.

The 2021 South Sandwich Island M_w 8.2 earthquake: a slow event sandwiched between regular ruptures

Zhe Jia[1], Zhongwen Zhan[1], Hiroo Kanamori[1]

[1]Seismological Laboratory, California Institute of Technology, Pasadena, CA 91125, USA.

Corresponding author. Zhe Jia (zjia@gps.caltech.edu)

Key Points

- The South Sandwich Island M_w 8.2 earthquake appears to have extended deep depth, yet displayed tsunami earthquake-like features.
- Inversions including long-period data revealed a M_w 8.16 slow subevent at shallow depth, connecting regular deep ruptures at the ends.
- The hybrid of deep and shallow ruptures represents an extreme example of the broad spectral behaviors of subduction zone earthquakes.

Abstract

We determined the rupture sequence of the Aug 12, 2021 M_w 8.2 South Sandwich Island earthquake which, according to the reports from the National Earthquake Information Center, appears to be a complex sequence in both time and space. Notable tsunamis were recorded by tide gauges at global distances. Given the complexity of this event, we used a multiple subevent inversion method that can accommodate complex variations of fault geometry, location, depth, and temporal characteristics of the event. We found that the rupture initiated as a regular deep thrust earthquake; it then triggered a shallow dominantly slow subevent extending ~200 km to the south, and ended with 2 other regular subevents. The total duration is ~260s, unusually long for an M_w 8.2 event. Our result is qualitatively consistent with other moment tensor solutions and the observed m_B-M_w and M_S-M_w relations, and provides a more quantitative space-temporal pattern of this unusual sequence.

Plain Language Summary

The 2021 August South Sandwich Island M_w 8.2 earthquake was a surprise, because it was initially reported as a magnitude 7.5 event at a deep depth (47 km) but generated a global-spreading tsunami that would only be expected for a larger and shallower event. By using seismic data with period as long as 500s, we revealed a hidden M_w 8.16 shallow slow event that happened between clusters of regular ruptures in the beginning and end. Although the slow event contributed 70% of the seismic moment, lasted three minutes, and ruptured a 200-km section of the plate interface, it is essentially invisible at short or intermediate periods, which explains its anomalously low body-wave and surface-wave magnitudes. The 2021 South Sandwich Island earthquake represents an extreme example of the broad spectral behaviors of subduction zone earthquakes and calls for attention in the research and warning of similar events.

1 Introduction

Large megathrust earthquakes on the subduction interface extend from near-trench to depths and display very different depth-varying slip behaviors [*Lay et al.*, 2012]. Large earthquakes that rupture the shallowest portion of the subduction interface (<15km) can generate devastating tsunamis, but they appear to rupture slowly with inefficient excitation of short-period seismic waves disproportionally to their seismic moment and tsunami. These earthquakes are "tsunami earthquakes" [*Kanamori*, 1972]. At deeper depths (15~50km), large thrust earthquakes have faster rupture velocities and stronger radiation of short-period seismic energy with inefficient tsunami generation. Their contrasting rupture characteristics are well interpreted by two distinct types of fault properties; the slow slip of shallow tsunami earthquakes is commonly attributed to weak sediments, while the brittle failures of unstable fault patches explain the fast deeper earthquakes.

On August 12, 2021, a great earthquake (M_w >8) struck the South Sandwich Island region of the south Atlantic Ocean (Fig. 1a). This event occurred close to the South Sandwich trench, where the South American plate subducts beneath the South Sandwich plate at a velocity of 7 cm/year [*Pelayo and Wiens*, 1989]. A remarkable observation of this earthquake is its far reaching-tsunamis. The tsunamis spread to the north Atlantic, Pacific, and Indian Oceans, where tide gauges measured peak amplitudes of ~20 cm at over 10,000 km distance from the source (Fig. S1). Although modeling these tide gauge observations is challenging because of the lack of detailed bathymetry data between the source and gauges, the observed tsunamis at global distances appear to suggest that the South Sandwich Island earthquake could be categorized as a regular shallow tsunamigenic earthquake.

However, the South Sandwich Island earthquake seems to have extended to large depths with a complex temporal history. The early report (PDE) from the National Earthquake Information Center (NEIC) of the US Geological Survey listed 2 events within 3 minutes: 1. NEIC1, At

18:32:52 (UTC) (25.03 °W, 57.68 °S, Depth=47.2 km, M_w=7.5) and 2. NEIC2, At 18:35:17 (25.26 °W, 58.38 °S, Depth=22.8 km, M_w=8.1). In this paper, we call collectively the earthquake sequence which started at 18:32:52 (UTC) and lasted for about 300s, the 2021 South Sandwich Island earthquake, and we refer the 1st (NEIC1) and 2nd (NEIC2) events as the foreshock and the mainshock, respectively. The Global Centroid Moment Tensor Project (GCMT) [*Ekström et al.*, 2012] reported 2 events: 1. GCMT1 (202108121832A, centroid time: 18:35:25, M_w=8.3, 24.34 ° W, 59.48 °S, Depth=20.0 km) and 2. GCMT2 (202108121835A, centroid time: 18:36:13, M_w=7.9, 25.15 °W, 60.47 °S, 15.1 km). USGS NEIC also reported a moment tensor solution at the centroid time around 18:36 with M_{wc}=7.98 and depth=10 km with an alternative solution with M_{ww}=8.13 and depth=35.5 km (more details in supporting table S1). Given the variability of these solutions, we attempted W-phase inversion. Because of the complex interference of the waveforms of several events, only with a very narrow long-period pass band (0.00125 to 0.002 Hz, i.e., 500 to 800 s), we could obtain a solution that can fit long-period waveforms satisfactorily for 40 stations (more details in supporting text S1, Fig. S2-3).

The depths reported by different catalogs range from 10 to 50 km, and the hypocenters scatter around the Slab 2.0 [*Hayes et al.*, 2018] interface (Fig. 1b). This is probably caused by difficulty in locating the events accurately, due to the complex interference of seismic waves from the foreshock and mainshock. Nevertheless, the deeper depths of the South Sandwich Island earthquake appear to contradict the shallow slip inferred from the global-spreading tsunami. While detailed rupture analyses would be needed to understand this disparity, it is difficult to define a physical fault plane for slip inversions due to the diverse locations and focal mechanisms from different sources (Fig. 1). In addition, the aftershocks extend ~400km along the curved subduction zone, making a planar fault unphysical. Thus, we need to analyze the rupture properties of this earthquake with flexibility in fault geometries, while maintaining the depth-dependent complexities.

In this study, we first investigate the overall spectral characteristics of the event. Then, we determine the kinematic rupture process with a multiple subevent inversion of broad-band seismic waveforms, and evaluate the contributions of subevents and discuss their relationships.

2 General Spectral Characteristics

Given the complex rupture characteristics of the 2021 South Sandwich Island earthquake, we first investigate this event using 3 magnitude scales, m_B, M_S, and M_w. Although m_B and M_S are old somewhat qualitative parameters, they are available for global earthquakes and useful for understanding the spectral characteristics of the South Sandwich Island sequence in global context. To the first order, m_B, M_S, and M_w represent the spectral amplitudes of the sequence at about 4s, 20s, and 200s or even longer period.

2.1 m_B vs. M_w relationship

For the measurement of m_B, we used the method described in Kanamori and Ross [2019] which follows the method developed by Gutenberg and Richter [1956]. We used the vertical component P-wave recorded at 54 global network stations (epicentral distance of 30 °-80 °, Fig. S4). The medians of station m_B are 6.87 and 7.10 for the foreshock and the mainshock, respectively. Fig. 2a compares the m_B-M_w relationship for these events with the m_B values of about 3,000 events with $M_w \geq 6$ for a period from 1988 to 2018 taken from Kanamori and Ross [2019]. The m_B data for the global events shown by small dots represent the range for ensemble of global events. The m_B for the mainshock is probably the upper bound because the time window for the m_B measurements contains some energy from the foreshock, only 145s earlier. The m_B values for the foreshock and the mainshock are 0.4 and 0.6 m_B unit, respectively, smaller than the average

111 global m_B-M_w trend; this indicates that these events, especially the mainshock, are deficient in
112 short-period energy.

113

114 **2.2 M_S vs. M_w relationship**

115 We made a similar comparison of M_S vs. M_w relationship. We computed M_S using 20 s surface
116 waves from 483 global seismic stations (distance range of 30°-120°), and measured the peak
117 ground motion amplitudes. Since the surface waves of the foreshock and mainshock overlap, we
118 could not measure M_S for each event separately, and obtained just one M_S=7.68 (Fig. S5).
119 Compared with the empirical global M_S-M_w relationship [*Di Giacomo et al.*, 2015] from the ISC
120 M_S dataset [*ISC*, 2021], the observed M_S is 0.5 smaller than the average trend (Fig. 2b).

121 The smaller m_B and M_S than the global average trends indicate depleted seismic energy release at
122 short periods and slow rupturing characteristics [*Kanamori*, 1972; *Kanamori and Ross*, 2019]. As
123 shown in Fig. 2a-b, the South Sandwich Island earthquake is among the biggest outliers from the
124 general trend. Other anomalous events similar to the South Sandwich Island earthquake includes
125 the 1992 Nicaragua M_w 7.6, the 1994 Java M_w 7.8, the1996 Peru M_w 7.5, the 2006 M_w 7.7 Java,
126 and the 2010 M_w 7.8 Mentawai Island earthquakes, all of which are well-known shallow slow
127 tsunami earthquakes. This similarity suggests that the South Sandwich Island earthquake
128 probably involved a substantial slow rupture component at the shallow subduction interface.

129

130 **3 Multiple subevent inversion**

131 To image the detailed rupture process of the earthquake, we applied the multiple subevent
132 inversion method. Our subevent inversion algorithm represents a complex rupture with multiple
133 simpler sources, each of which can have different timings, locations, source durations and focal

mechanisms [*Jia et al.*, 2020a; *Jia et al.*, 2020b; *Ross et al.*, 2019; *Zhan et al.*, 2014]. This simple parameterization allows flexible representation of time history and fault geometries, thereby capturing the first-order spatiotemporal rupture complexities. Our subevent method is particularly suitable for describing the South Sandwich Island earthquake which contains at least two major events in 3 minutes and involves potential fault geometry variations along the curved South Sandwich trench. As the possible slow rupture may propagate long distance with strong directivity effects, we introduce a finite subevent with a unilateral Haskell rupture model with a constant rupture velocity [*Haskell*, 1964]. In this study, we use the Haskell model only for the long duration (>100s) subevent with potentially significant rupture directivity. We applied a Markov Chain Monte Carlo inversion in a Bayesian framework, and increased the number of subevents iteratively until the waveforms fit well (supporting text S2 for more details).

We collected 58 teleseismic (distance of 30°-90°) P velocity and displacement records, 43 teleseismic SH displacement records, and 12 three-component regional (distance within 40°) full waveforms in displacement (Fig. S6) for the subevent inversion. We removed their instrumental responses, and filtered the P and SH waves between 0.005-0.05 Hz for modeling short period features. For the regional full waves, we used them in two datasets with different filter bands. One of them with a 0.002-0.02 Hz passband represents intermediate period waves, and the other with 0.002-0.0033 Hz, long period motions. This combination of short, intermediate and long period bands allows mapping the ruptures of different length scales simultaneously. The teleseismic Green's functions are calculated combining the propagator matrix method and plane wave approximation [*Kikuchi and Kanamori*, 1991; *Qian et al.*, 2017], using the CRUST 2.0 [*Laske et al.*, 2001] model at the source region and the IASPEI91 model [*Kennet*, 1991] at other places. The regional full-wave synthetics are computed with a frequency-wavenumber integration algorithm [*Zhu and Rivera*, 2002], using the PREM model [*Dziewonski and Anderson*, 1981].

158 Our subevent model consists of 5 subevents that span ~300 km along the trench (Fig. 3,
159 supporting table S2). We fixed the first subevent at the NEIC M_w 7.5 event hypocenter. Data
160 fittings (Fig. 3b, Fig. S7) and model uncertainties (Fig. S8) suggest that the source parameters are
161 well constrained. The rupture begins with two short-duration subevents E1 (centroid time τ_C=13s
162 after the origin time, duration d_C=23s, M_w 7.2) and E2 (τ_C=36s, d_C=19s, M_w 7.2), which in total
163 (M_w 7.4) generally represents the NEIC M_w 7.5 foreshock. They have close locations and similar
164 shallow dipping thrust focal mechanisms (average strike/dip/rake=157°/18°/82°), but the centroid
165 depth of E1 is deep (39 km) while E2 is shallow (7 km), suggesting an up-dip rupture propagation
166 along the plate interface. They are located near a patch of dense aftershock seismicity (Fig. 3a).

167 Concurrent with the rupture initiation represented by E1-E2 in the first 50 s, the subevent E3
168 (τ_C=90s, M_w 8.16) emerged and continued for ~180 s. E3 contributes the most seismic moment of
169 the South Sandwich Island earthquake, and its moment rate function (Fig. 3c) has a remarkably
170 smaller aspect ratio (peak moment rate over duration, $1.2*10^{17}$ N-m/s^2) than regular subevents
171 E1-E2 (average of $3.3*10^{17}$ N-m/s^2). As a Haskell source, E3 initiates close to the locations of
172 E1-E2, and unilaterally propagates towards the south with a slow velocity (~1 km/s) and a long
173 fault length (~180 km). E3 is located at 14 km depth with an uncertainty of ±5 km (Fig. S8), and
174 it has a very shallow-dipping thrust mechanism (strike/dip/rake=134°/4°/22°), although the strike
175 and rake angles are not well constrained due to the shallow dip angle (Fig. S9). The shallow slow
176 slip of E3 presumably transfers the stress along the slab, which explains the downdip dense
177 aftershock seismicity as well as the triggered outer-rise earthquakes (Fig. 3).

178 The rupture terminated with the final two subevents E4 (τ_C=195s, d_C=26s, M_w 7.6) and E5
179 (τ_C=226s, d_C=50s, M_w 7.7) at 250-300 km south of the epicenter. They occurred about 3 minutes
180 after the rupture initiation. E4 and E5 are also shallow dipping thrust subevents (average
181 strike/dip/rake=206°/23°/106°), but their strike angles are ~50 degrees rotated clockwise from
182 E1-E2. This rotation is consistent with the geometry of the curved South Sandwich Island trench.

Their locations are close to the downdip high-density aftershock patch (Fig. 3). This spatial pattern is similar to that for the other two major slip asperities (E1-E2 and E3). The depth of E4 (25 km) is significantly deeper than E5 (9 km), indicating coexisting megathrust slip at different depth domains. Moment rate functions of E4-E5 display similar aspect ratios (average of $5.3*10^{17}$ N-m/s^2) to E1-E2, indicating that E4 and E5 are, unlike E3, more like regular ruptures.

The low aspect ratio, slow rupture velocity, overall shallow depth, and shallow-dipping mechanism of E3 suggest that it is a "slow earthquake" at the shallow subduction interface. This feature can be most prominently demonstrated in Fig. 4. The regular subevents E1, E2, E4 and E5 contribute almost all of the short and intermediate period waveforms, while E3 barely excited short and intermediate period signals (Fig. 4a-4c, Fig. S10). In contrast, E3 generated large long-period waves, comparable to the sum of all other subevents (Fig. 4d, Fig. S10). The diminished short period excitation explains the smaller-than-average m_B and M_S of E3 (Fig.2).

Fig. 3c compares the overall rupture sequence determined by our multiple subevent inversion with the events determined by other methods. The sequence starts with E1 which is the foreshock (NEIC1). The long duration subevent E3 connects the short duration subevents E1-E2 at the beginning and E4-E5 at the end, forming a continuous megathrust rupture process. This approximately corresponds to the long-duration GCMT1 (M_w 8.3) in the middle of the rupture extent (Fig. 1). The GCMT2 (M_w 7.9, half duration=24 s), with the centroid time 48 s later than GCMT1 probably overlaps with GCMT1 in time, and roughly corresponds to E4-E5 at the southern tip with rotated strike angles (Fig. 1). The W-phase solution, which is similar to the NEIC M_{ww}, probably represents a very long-period component of the latter half of the sequence (Fig. 1, Fig. S2).

4 Discussion and conclusions

The 2021 South Sandwich Island (M_w 8.2) earthquake is a complex multiple event, including a slow subevent E3 connecting other regular thrust subevents at the beginning and the end. The slow subevent E3 contributes 70% of the total seismic moment of the sequence. The large moment and the relatively shallow depth of E3, with weak short-period seismic radiation, make this sequence as a whole look like a tsunami earthquake. The total duration of the whole sequence (E1 to E5) is about 260s; thus, the centroid time shift, 130s, estimated from the half duration is anomalously long on the centroid time delay vs. M_w scaling relation obtained by [*Duputel et al.*, *2013*], as shown by Fig. 5. The 2002 Guerrero earthquake [*Kostoglodov et al.*, 2003] and the 2006 Java earthquake [*Ammon et al.*, 2006], both of which are slow tsunami earthquakes, share a similar trend on Fig. 5. Thus, the South Sandwich Island earthquake appears to be a hybrid of deep rupture and slow tsunamigenic slip; this explains the somewhat unusual combination of the relatively large depth and the globally-observed tsunami.

Although the shallowest subduction interface is often considered seismically inactive due to the velocity-strengthening frictional properties [*Scholz*, 1998], some large tsunami earthquakes were found to host major slip at near-trench depths [*Kanamori and Kikuchi*, 1993; *Lay et al.*, 2011]. However, the slow component of the South Sandwich Island earthquake may have a broader depth extent than the traditional tsunami earthquakes. The slow subevent E3 has an overall shallow centroid depth of 14 km, which explains its global-spreading tsunamis and the two large (~M_w 7) outer-rise aftershocks (Fig. 1) due to the possible stress transfer at shallow subduction interface [*Sladen and Trevisan*, 2018]. However, it is probably not confined in the near-trench depths like other tsunami earthquakes, but could have extended to deeper domains, which is consistent with absence of observation of devastating tsunami. The deeper slip could trigger slow rupture by dynamic weakening [*Ma*, 2012; *Noda and Lapusta*, 2013], making the slip span over a broad depth range. However, the detailed depth distribution of the slow subevent remains unclear

and difficult to resolve, because of the tradeoff between seismic moment, dip angle and depth [*Tsai et al.*, 2011]. This requires further investigations.

In summary, the 2021 South Sandwich Island M_w 8.2 earthquake involves a complex depth-varying rupture process. The complex interaction of deep regular slip and shallow slow subevent explains somewhat contradicting combination of the deep subevents, the tsunami earthquake-like features with diminished short-period seismic radiation and the global-spreading tsunamis. This highlights the importance of accurately mapping the slow components of megathrust earthquakes over a broad frequency band for reliable tsunami warning.

Acknowledgments

We thank the IRIS for providing public access (http://ds.iris.edu/wilber3/find_event) to all the seismic data. We thank the IOC of UNESCO for providing public access (http://www.ioc-sealevelmonitoring.org/) to the tide gauge data. This work is supported by USGS grant G19AP00030.

Data Availability Statement

All figures are plotted using GMT (https://www.generic-mapping-tools/) and MATLAB (http://www.mathworks.com/) software. Seismic data are available on the IRIS Wilber 3 page (https://ds.iris.edu/wilber3/find_stations/11455082). Tide gauge data are available on the IOC sea level page (http://www.ioc-sealevelmonitoring.org/list.php).

References

Ammon, C. J., H. Kanamori, T. Lay, and A. A. Velasco (2006), The 17 July 2006 Java tsunami earthquake, *Geophys. Res. Lett.*, *33*(24).

Di Giacomo, D., I. Bondár, D. A. Storchak, E. R. Engdahl, P. Bormann, and J. Harris (2015), ISC-GEM: Global Instrumental Earthquake Catalogue (1900–2009), III. Re-computed MS and mb, proxy MW, final magnitude composition and completeness assessment, *Phys. Earth Planet. Inter.*, *239*, 33-47.

Duputel, Z., V. C. Tsai, L. Rivera, and H. Kanamori (2013), Using centroid time-delays to characterize source durations and identify earthquakes with unique characteristics, *Earth Planet. Sci. Lett.*, *374*, 92-100, doi:10.1016/j.epsl.2013.05.024.

Dziewonski, A. M., and D. L. Anderson (1981), Preliminary reference Earth model, *Phys. Earth Planet. Inter.*, *25*(4), 297-356.

Ekström, G., M. Nettles, and A. Dziewoński (2012), The global CMT project 2004–2010: Centroid-moment tensors for 13,017 earthquakes, *Phys. Earth Planet. Inter.*, *200*, 1-9.

Gutenberg, B. and C.F. Richter (1956), Earthquake magnitude, intensity, energy, and acceleration: (Second paper). *Bulletin of the seismological society of America*, *46*(2), pp.105-145.

Haskell, N. (1964), Total energy and energy spectral density of elastic wave radiation from propagating faults, *Bull. Seismol. Soc. Am.*, *54*(6A), 1811-1841.

Hayes, G. P., G. L. Moore, D. E. Portner, M. Hearne, H. Flamme, M. Furtney, and G. M. Smoczyk (2018), Slab2, a comprehensive subduction zone geometry model, *Science*, *362*(6410), 58-61.

International Seismological Centre, . (2021). The ISC MS dataset for shallow earthquakes since 1904, *ISC Seismological Dataset Repository*, https://doi.org/10.31905/0N4HOS2D

Jia, Z., Z. Shen, Z. Zhan, C. Li, Z. Peng, and M. Gurnis (2020a), The 2018 Fiji Mw8.2 and 7.9 deep earthquakes: One doublet in two slabs, *Earth Planet. Sci. Lett.*, *531*, 115997.

Jia, Z., X. Wang, and Z. Zhan (2020b), Multifault Models of the 2019 Ridgecrest Sequence Highlight Complementary Slip and Fault Junction Instability, *Geophys. Res. Lett.*, *47*(17), e2020GL089802.

Kanamori, H. (1972), Mechanism of tsunami earthquakes, *Phys. Earth Planet. Inter.*, *6*(5), 346-359.

Kanamori, H., and M. Kikuchi (1993), The 1992 Nicaragua earthquake: a slow tsunami earthquake associated with subducted sediments, *Nature*, *361*(6414), 714-716.

Kanamori, H., and L. Rivera (2008), Source inversion ofWphase: speeding up seismic tsunami warning, *Geophys. J. Int.*, *175*(1), 222-238.

Kanamori, H., and Z. E. Ross (2019), Reviving m B, *Geophys. J. Int.*, *216*(3), 1798-1816.

Kennet, B. (1991), IASPEI 1991 seismological tables, *Terra Nova*, *3*(2), 122-122.

Kikuchi, M., and H. Kanamori (1991), Inversion of complex body waves—III, *Bull. Seismol. Soc. Am.*, *81*(6), 2335-2350.

Kostoglodov, V., S. K. Singh, J. A. Santiago, S. I. Franco, K. M. Larson, A. R. Lowry, and R. Bilham (2003), A large silent earthquake in the Guerrero seismic gap, Mexico, *Geophys. Res. Lett.*, *30*(15).

Laske, G., G. Masters, and C. Reif (2001), CRUST 2.0: A new global crustal model at 2×2 degrees, *Institute of Geophysics and Planetary Physics, The University of California, San Diego, website http://mahi. ucsd. edu/Gabi/rem. dir/crust/crust2. html*.

Lay, T., C. J. Ammon, H. Kanamori, Y. Yamazaki, K. F. Cheung, and A. R. Hutko (2011), The 25 October 2010 Mentawai tsunami earthquake (Mw7.8) and the tsunami hazard presented by shallow megathrust ruptures, *Geophys. Res. Lett.*, *38*(6).

Lay, T., H. Kanamori, C. J. Ammon, K. D. Koper, A. R. Hutko, L. Ye, H. Yue, and T. M. Rushing (2012), Depth-varying rupture properties of subduction zone megathrust faults, *J. Geophys. Res.*, *117*(B4), doi:10.1029/2011jb009133.

Ma, S. (2012), A self-consistent mechanism for slow dynamic deformation and tsunami generation for earthquakes in the shallow subduction zone, *Geophys. Res. Lett.*, *39*(11).

Noda, H., and N. Lapusta (2013), Stable creeping fault segments can become destructive as a result of dynamic weakening, *Nature*, *493*(7433), 518-521.

Pelayo, A. M., and D. A. Wiens (1989), Seismotectonics and relative plate motions in the Scotia Sea region, *Journal of Geophysical Research: Solid Earth*, *94*(B6), 7293-7320.

Qian, Y., S. Ni, S. Wei, R. Almeida, and H. Zhang (2017), The effects of core-reflected waves on finite fault inversions with teleseismic body wave data, *Geophys. J. Int.*, *211*(2), 958-973.

Ross, Z. E., B. Idini, Z. Jia, O. L. Stephenson, M. Zhong, X. Wang, Z. Zhan, M. Simons, E. J. Fielding, and S.-H. Yun (2019), Hierarchical interlocked orthogonal faulting in the 2019 Ridgecrest earthquake sequence, *Science*, *366*(6463), 346-351.

Scholz, C. H. (1998), Earthquakes and friction laws, *Nature*, *391*(6662), 37-42.

Sladen, A. and J. Trevisan (2018). Shallow megathrust earthquake ruptures betrayed by their outer-trench aftershocks signature. *Earth and Planetary Science Letters*, *483*, pp.105-113.

Tsai, V. C., G. P. Hayes, and Z. Duputel (2011), Constraints on the long-period moment-dip tradeoff for the Tohoku earthquake, *Geophys. Res. Lett.*, *38*(7).

Zhan, Z., H. Kanamori, V. C. Tsai, D. V. Helmberger, and S. Wei (2014), Rupture complexity of the 1994 Bolivia and 2013 Sea of Okhotsk deep earthquakes, *Earth Planet. Sci. Lett.*, *385*, 89-96.

Zhu, L., and L. A. Rivera (2002), A note on the dynamic and static displacements from a point source in multilayered media, *Geophys. J. Int.*, *148*(3), 619-627.

Figures

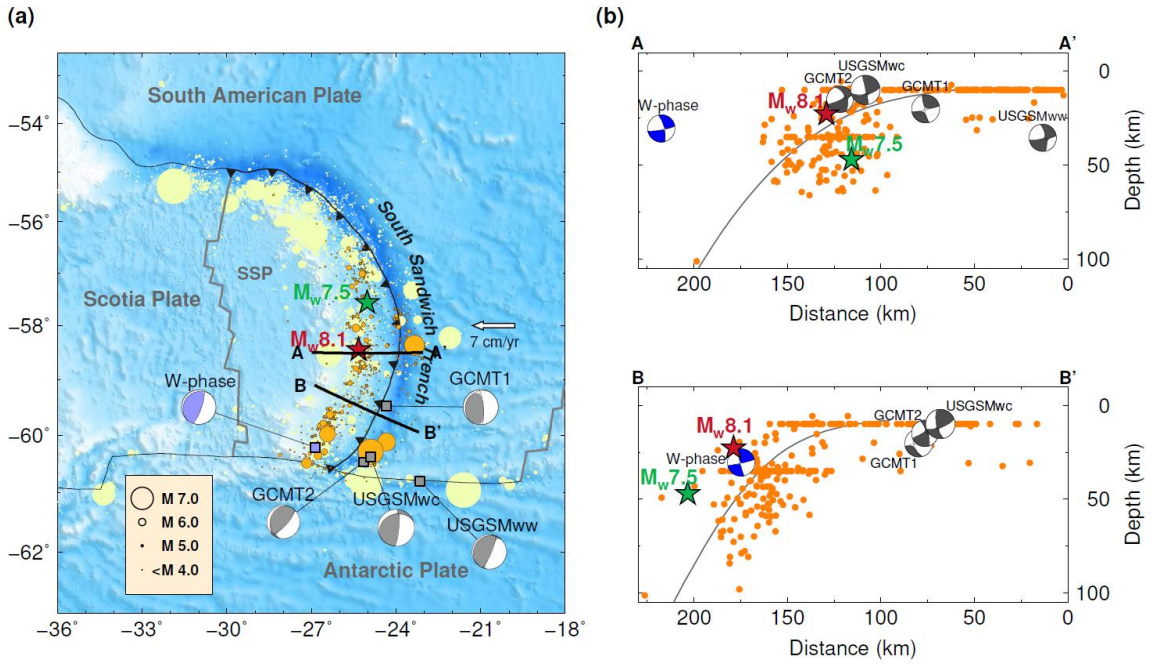

Figure 1. Overview of the tectonic setting and seismicity. (a) Tectonics of the South Sandwich region. The M_w 7.5 foreshock (green star) and the M_w 8.1 mainshock (red star) occurred close to the South Sandwich Trench, where the South America Plate subducts under the South Sandwich Plate (SSP). Yellow circles show the background seismicity according to the ISC catalog. Orange circles indicate the aftershocks within two weeks of the South Sandwich event. The beachballs display our W-phase moment tensor (in blue), USGS NEIC M_{wc}, M_{ww}, and two Global CMT solutions (in gray). (b) Cross-sections along the black line segments in (a). The orange dots indicate the aftershocks within 100 km of the profiles. The black line represents the Slab 2.0 interface. Beachballs and stars are the same as (a), but for cross section views.

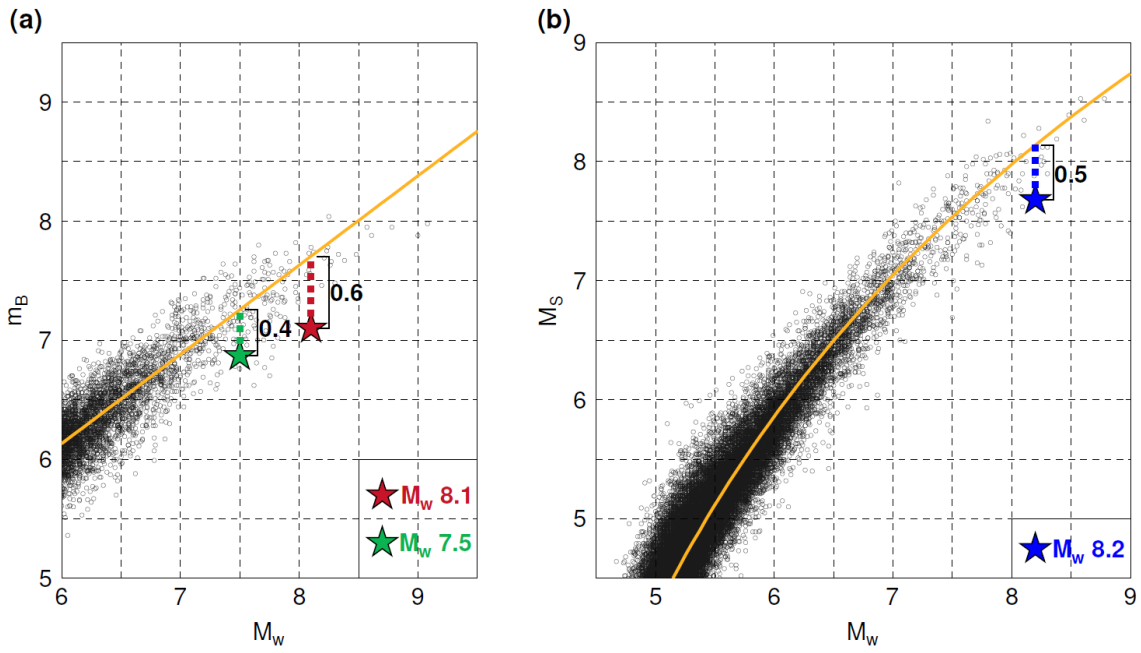

Figure 2. m_B and M_S measurements for the South Sandwich Island sequence. (a) Body wave magnitude m_B for the M_w 7.5 foreshock (green star) and the M_w 8.1 mainshock (red star). The solid yellow line indicates the general trend, m_B=0.75 M_w +1.63 [*Kanamori and Ross*, 2019], which is regressed from the database of global earthquakes for the period 1988-2018 (black circles). (b) Surface wave magnitude M_S for the sequence. The solid yellow line shows the empirical relation, $M_w = \exp(-0.222+0.233M_S)+2.863$, regressed from the historical earthquakes (black circles) in the GCMT catalog [*Di Giacomo et al.*, 2015].

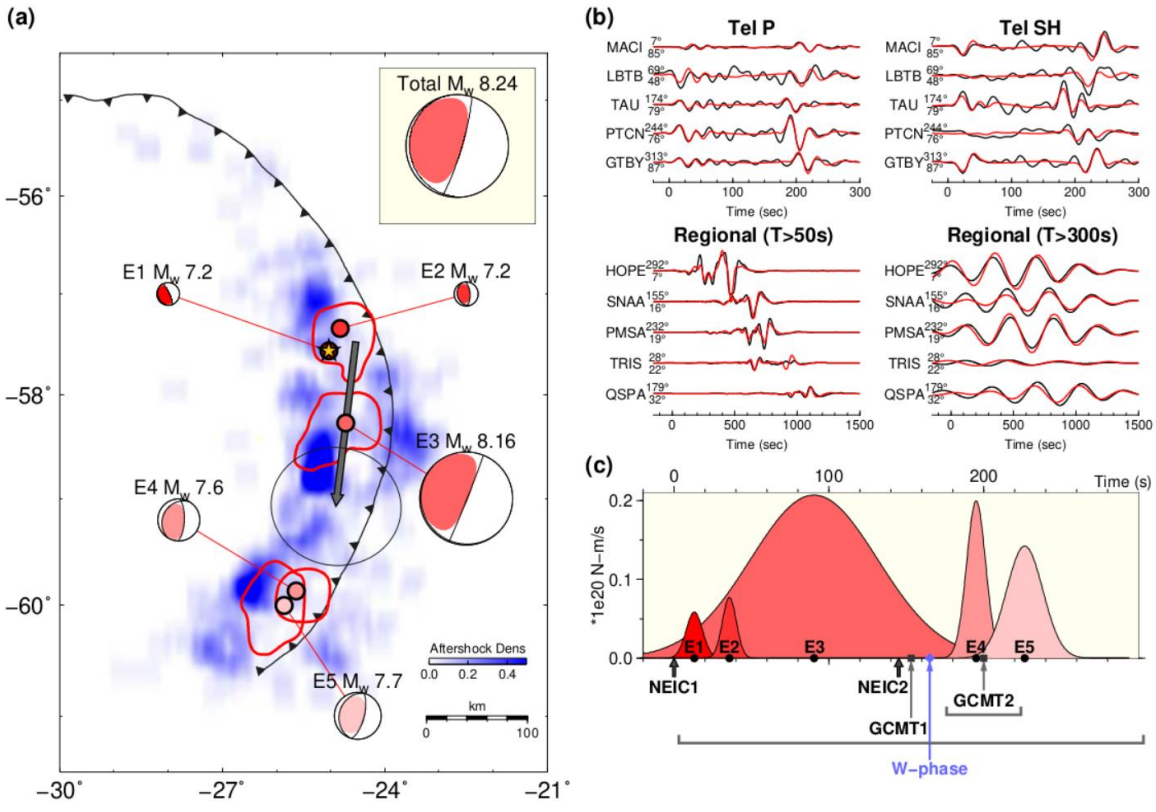

Figure 3. Rupture process of the South Sandwich Island sequence. (a) Subevent locations (red dots) and focal mechanisms (red beachballs). Yellow star indicates the hypocenter, collocated with the first subevent E1. The red contours show 95% confidence limits of the subevent locations. The gray arrow at E3 indicates its rupture directivity, and its length reflects rupture length. The black contour at the arrow end shows the 95% confidence limit of the rupture length and direction of E3, assuming the back end as the starting point. The aftershock density is displayed by the blue background color. The inset box shows the summation of subevent moment tensors. (b) Representative data (black) and synthetic (red) waveform fits for teleseismic P and SH waves (0.005-0.05 Hz), vertical component intermediate period (0.002-0.02 Hz) and long period regional (0.002-0.0033 Hz) full waves. The numbers leading the traces are azimuths and distances. (c) Moment rate functions for all subevents. The black circles indicate subevent centroid times. The dark arrows point to two NEIC event origin times. Gray squares and blue

357 diamond indicate centroid times of the GCMT and W-phase solutions, and the underneath solid
358 lines denote the corresponding source durations.

359

360

361

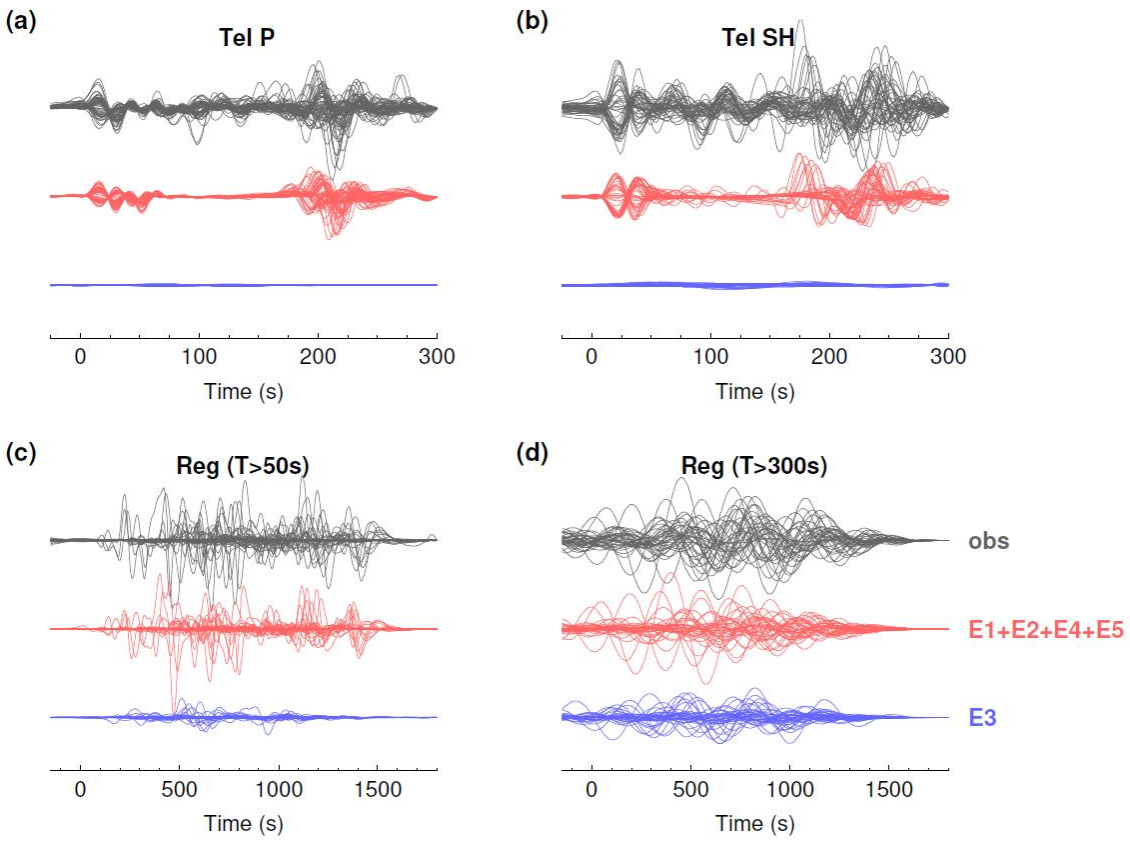

Figure 4. Waveform contributions from two groups of subevents. The observed data for all stations are plotted together in black lines. The total contribution from regular subevents E1, E2, E4, E5 are in red lines. The synthetics of the slow subevent E3 are indicated by blue lines. (a) P waves. (b) SH waves. (c) Intermediate period (0.002-0.02 Hz) and (d) long period (0.002-0.0033 Hz) regional full waveforms.

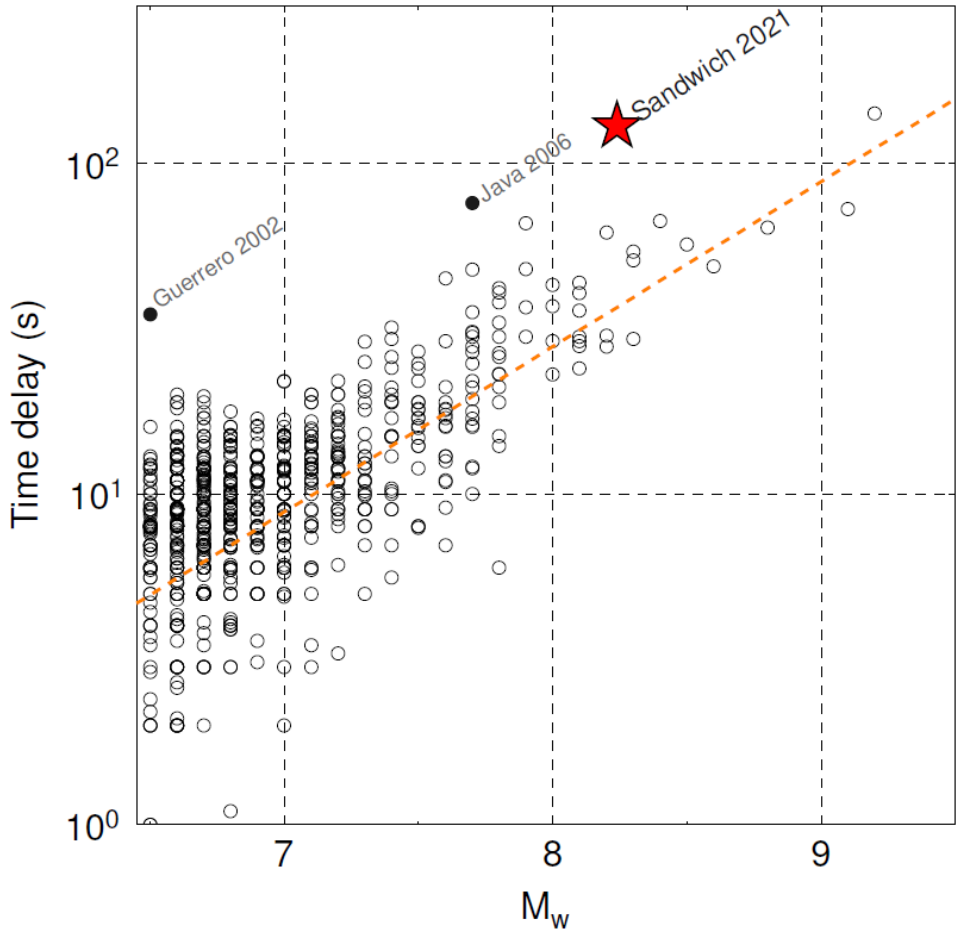

Figure 5. Relation between time delay (half duration) and M_w for the South Sandwich Island event (red star). Black circles represent the time delays of historical events from the W-phase measurements, the orange dashed line indicates an exponential relationship using the stress parameter of 0.37 MPa [*Duputel et al.*, 2013].

Geophysical Research Letters

Supporting Information for

The 2021 South Sandwich Island M_w 8.2 earthquake: a slow event sandwiched between regular ruptures

Zhe Jia[1*], Zhongwen Zhan[1], Hiroo Kanamori[1]

[1] Seismological Laboratory, California Institute of Technology, Pasadena, CA 91125, USA.

Contents of this file

Texts S1-S2
Figures S1 to S10
Table S1-S2

Introduction

This supporting information provides: two additional texts for the methods (Text S1-S2), 10 figures (Figure S1-S10), and two tables (Table S1-S2) to support the main text.

Text S1. W-phase inversion.

NEIC PDE listed 2 events:

8/12/2021 18:32:52 (UTC), depth=47.2 km, M_w=7.5

8/12/2021 18:35:17 (UTC), depth=22.8 km, M_w=8.1

These 2 events are only 145 s apart, and the standard W phase inversion for the 1st event could not converge at any reasonable solution because the W phases from the 2 events interfered. The standard inversion for the 2nd event did not work either for the same reason. For the 2nd event, only after several trials using different frequency bands, we could achieve a reasonable waveform fit with a relatively narrow low-frequency band 0.00125 to 0.002 Hz (*i.e.*, 500 to 800 s). This solution (Fig. S2) can fit the W phase waveforms reasonably well for 45 phases at 40 stations (Fig. S2). However, because of the very narrow band and the complex interference of phases, the centroid location, especially the depth, is poorly constrained (Fig. S3). The overall mechanism and size of the event seem to be reasonably well constrained. The centroid time shift, t_c, is 20 s from 18:35:17(UTC) which means that the centroid time of this event is 18:35:37(UTC) which is 165 s after the origin time of the 1st event. Thus we consider that this event approximately corresponds to the GCMT event 202108121832A (referred to as GCMT1, centroid time 18:35:25 UTC, M_w=8.3). However, the quality of the solution is not up to the standard W phase solution because of the complex waveform interferences of the multiple events of the sequence.

Text S2. Subevent inversion for the M_w 8.2 South Sandwich Island sequence.

We applied our subevent inversion method to simultaneously estimate the source parameters of 5 subevents. Each subevent has 10 point-source parameters, including 3 parameters for the subevent horizontal location and depth, a centroid time, a source time duration, and 5 deviatoric moment tensor elements. For the long-period subevent E3, we added two finiteness parameters, rupture velocity and rupture direction, to accommodate a Haskell unilateral rupture source with a constant rupture velocity. In this Haskell model, the dependence of the apparent source duration on rupture direction can be given by the following equation (local rise time is ignored),

$$D = D_0 \cdot \left(1 - \frac{V_r}{c} \cdot \cos(\theta - \varphi)\right)$$

, where D is the apparent source duration for a station of azimuth φ, D_0 is the rupture duration, V_r is the rupture velocity, c is the phase velocity, and θ is the rupture direction. In this study, we calculate phase velocities for teleseismic P and SH waves with ray tracing, using the IASPEI91 model. Because the regional full waveforms are dominated by surface waves, we assume c to be 4 km/s as approximate Rayleigh and Love phase velocities at a dominant period of 50s and 300s. Overall, this hybrid parameterization of point source and Haskell subevents has 52 unknown parameters.

To improve the searching efficiency, we divide our inversion procedure into two stages, where we search a part of these parameters nonlinearly and invert the data for other parameters in a linear way. The outer stage has a Markov Chain Monte Carlo (MCMC) inversion sampler that searches nonlinear parameters (subevent locations, centroid times, source durations, rupture velocity and rupture direction). Its random walk process to propose new models is driven by a Metropolis-Hasting algorithm. In each step, the model is proposed by perturbing one of the nonlinear parameters while keeping the other nonlinear parameter at their current values. This approach ensures a high acceptance rate and improves the efficiency of converging to the optimum. For each set of nonlinear parameters, we can linearly invert the data for the moment tensors of subevents as the inner stage, because the observed time series can be linearly related by subevent moment tensors and their Green's functions when subevent locations and timing are available. In practice, we predict apparent source time functions at all stations using the subevent locations and timings, then convolve them with the corresponding Green's functions, and eventually invert for deviatoric subevent moment tensors by extending the linear framework to multiple sources. In this way, only 27 nonlinear parameters are searched through the MCMC inversion, and it's much easier to extensively explore the model space.

We generated 72 Markov Chains and eventually kept 24 of them to avoid being trapped in local minima. The initial sample for each chain is randomly generated from bounded uniform distributions. Our MCMC inversion incorporates a Bayesian framework that propagates the data error and prior knowledge to the model error. We set the prior of all unknown parameters to be uniform distributions. We also empirically set the data error to be 10% to accommodate the inaccurate assumptions of the wave propagation processes, even though the true data error (noise and instrumental error) of the seismic waves are very small. This data error eventually turns to the width of the Markov Chain sample distributions, which reflects the posterior probability density functions.

We used 58 vertical component teleseismic (epicentral distance of 30°-90°) P waves in both displacement and velocity, 43 transverse component teleseismic SH waves in displacement, 12 three-component regional (epicentral distance within 40°) full waveforms in displacement in

our subevent inversion from the Global Seismic Network and the International Federation of Digital Seismograph Networks. The weighting of these three datasets is set to be 20:10:1 for similar final misfit contributions. For the inversion of teleseismic waves, we calculate the Green's functions with a hybrid method that combines propagator matrix and ray theory, and use a combination of the CRUST2.0 velocity model at the source location with an IASPEI91 model in the deeper earth. A limitation of this forward simulation method is that it does not consider PP or SS phases, but since the M_w 7.5 foreshock is much smaller than the M_w 8.1 mainshock, the PP and SS amplitudes of the foreshock do not overwhelm the P and S of the mainshock, the waveform interferences are limited. We also compute the regional full waveform synthetics with a frequency-wavenumber integration algorithm using the PREM model as an average structure from sea to land. We used the P and S arrival times predicted from ray tracing with the IASPEI91 model, and allowed maximum time shifts of 4s, 6s and 10s for the P, SH, and regional full waves. Because all subevents could move their horizontal locations together with the seismograms shifting simultaneously, we need to fix the horizontal location of one subevent. Therefore, we anchored the location of the first subevent E1 at the hypocenter of the M_w 7.5 foreshock, assuming the rupture dimension between the initiation and centroid of E1 is small compared with the full sequence.

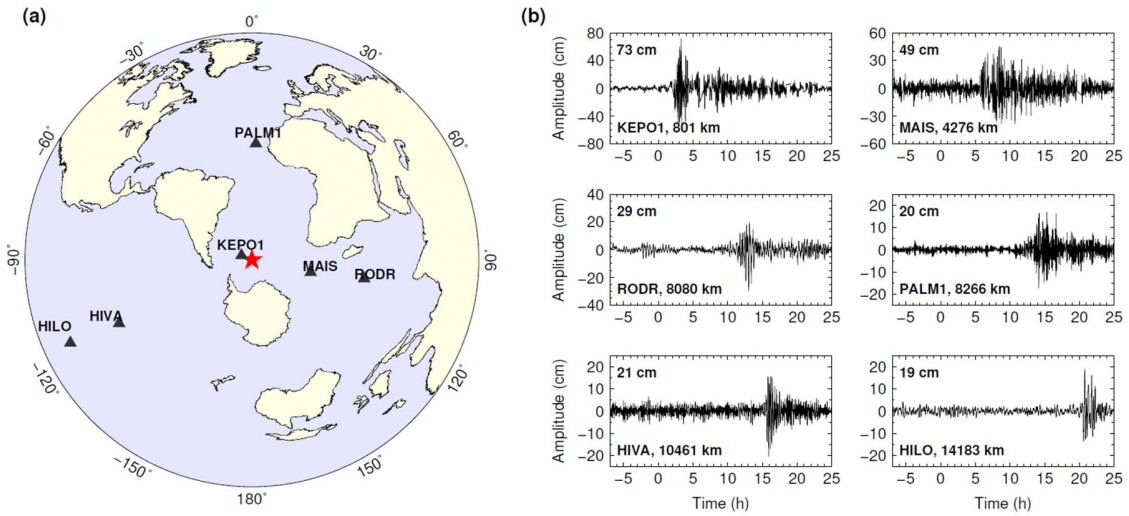

Figure S1. Tsunami of the South Sandwich Island sequence observed by tide gauges. (a) Distributions of the tide gauge stations (black triangles). The red star indicates the hypocenter of the South Sandwich Island sequence. (b) Waveforms recorded at the tide gauges in (a). The waveforms are high-pass filtered to periods shorter than 5 hours. The number above each trace shows the peak absolute amplitude of the tsunami. Below each trace the tide gauge station name and the distance from the South Sandwich Island earthquake source are shown.

(a)

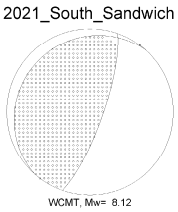

Moment Tensor [dyn-cm x 1e28]: 0.8130 -0.2078 -0.6052 0.5270 1.6134 -0.3721
Scalar moment [dyn-cm]: 1.89e+28
Best Nodal planes (strike/dip/rake): NP1 221.8/ 13.7/ 111.8 NP2: 19.4/ 77.3/ 84.8
Eigenvalues (dyn-cm x 1e28): 1.8945 -0.0185 -1.8760 (Mw = 8.12)
Fit Quality: RMS: 0.00343 mm (0.417) GAP: 93.9°, C# 724
Filter parameters: filt_order: 4 filt_cf1 : 0.00125 filt_cf2 : 0.00200 filt_pass : 1

(b)

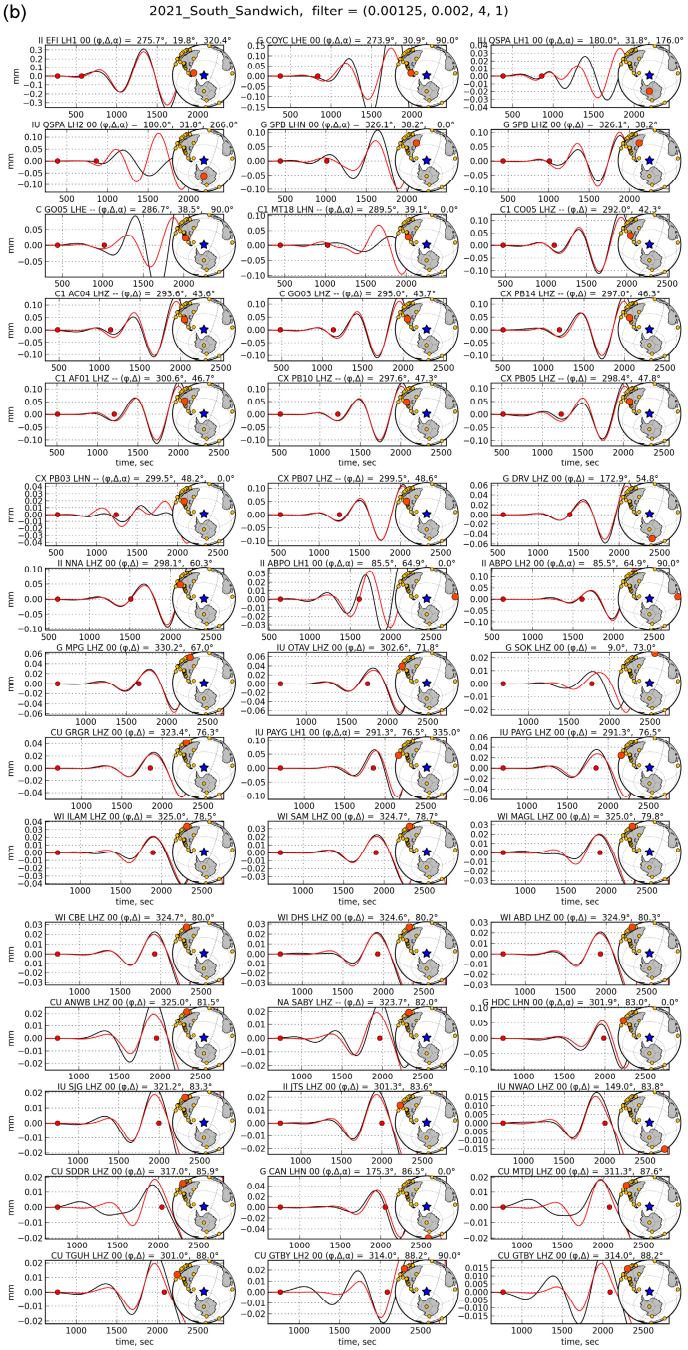

Figure S2. Long period W-phase point source solution for the 2021 South Sandwich Island sequence. (a) W-phase moment tensor and source parameters. The beachball shows the deviatoric moment tensor. The following lines display the moment tensor elements, scalar moment, and eigenvalues. The centroid depth is 30.5 km. (b) W-phase waveforms (between the red dots) for observation (black) and synthetics (red). Location of each station is indicated by the big red dot among the total set of stations used.

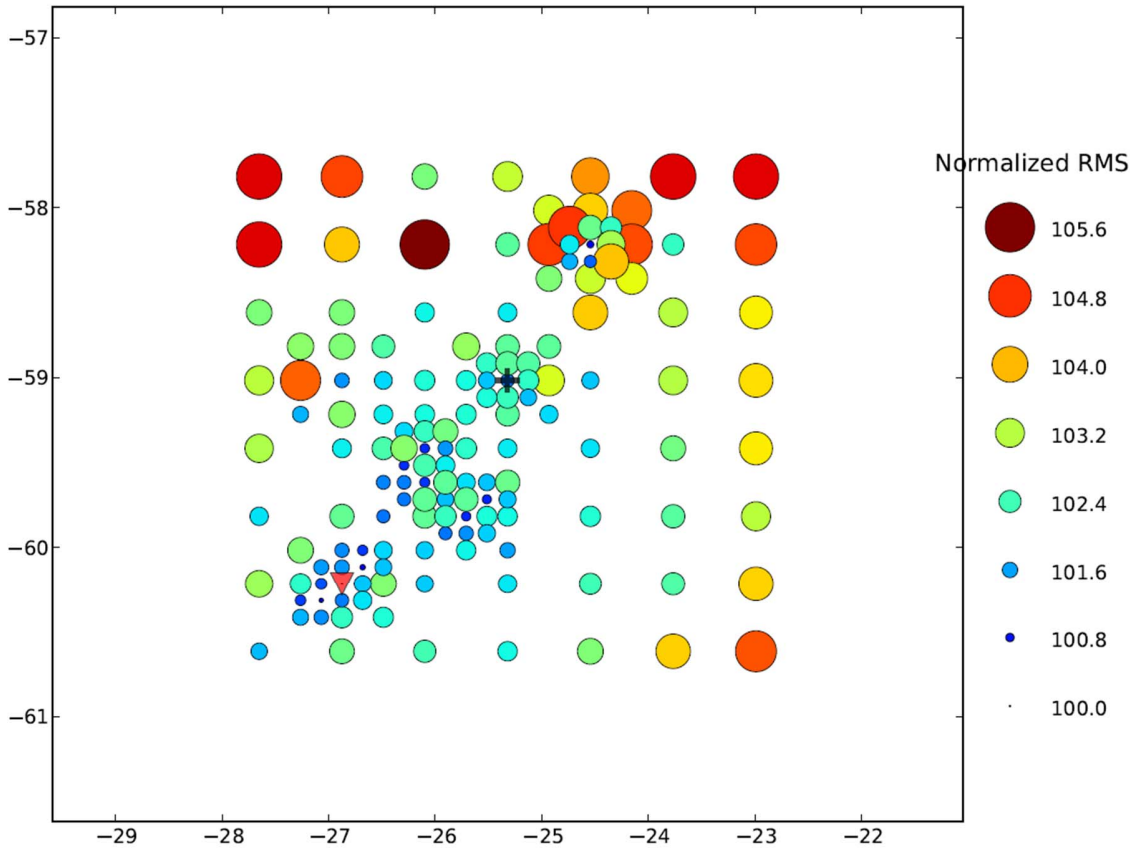

Figure S3. Resolution of location for the W-phase inversion. Circles indicate the searched locations. Their sizes and colors show the normalized root mean square misfit.

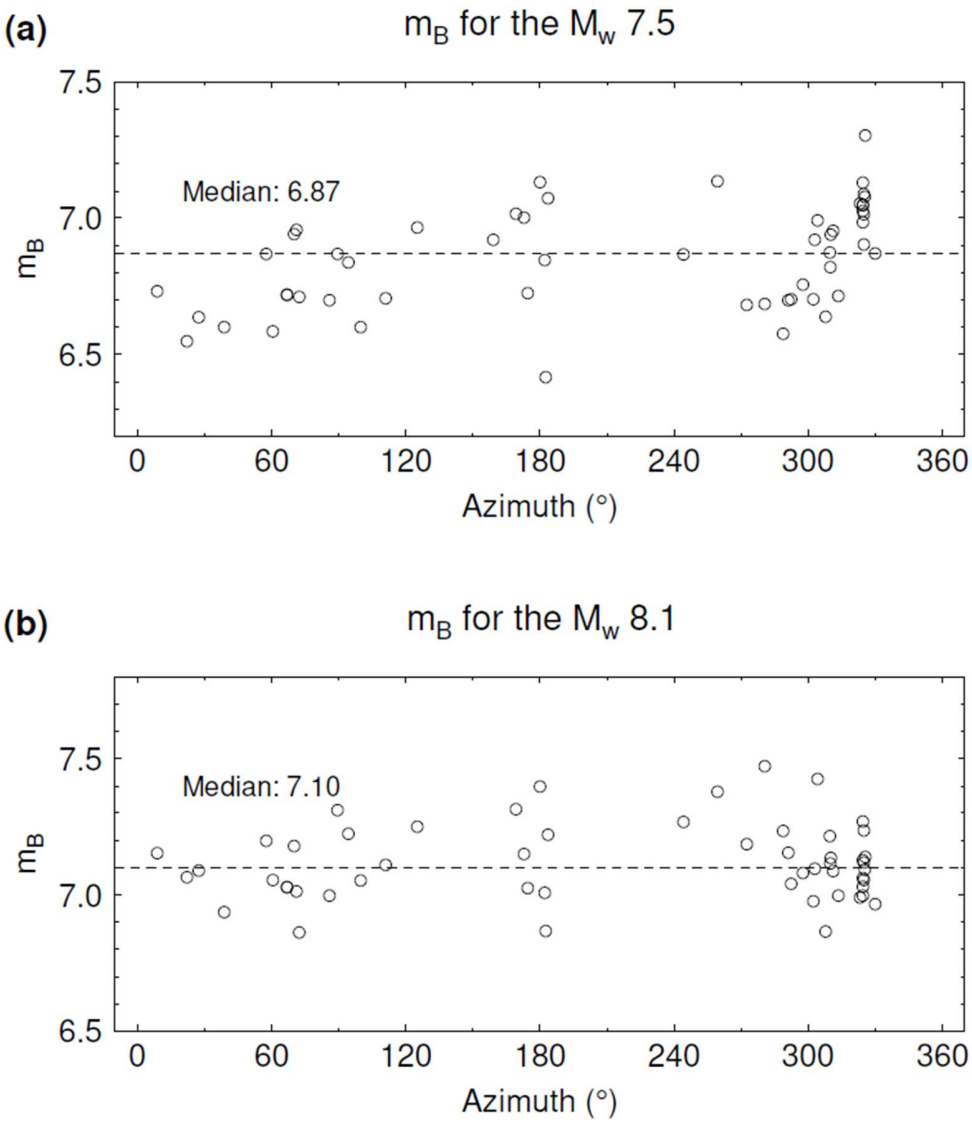

Figure S4. Body wave magnitudes of the South Sandwich Island sequence. (a) Individual body wave magnitudes m_B using stations at different azimuths (black circles) for the M_w 7.5 foreshock. The black dashed line shows the median m_B of 6.87. (b) Same as (a), but for the M_w 8.1 mainshock. The median m_B is 7.10.

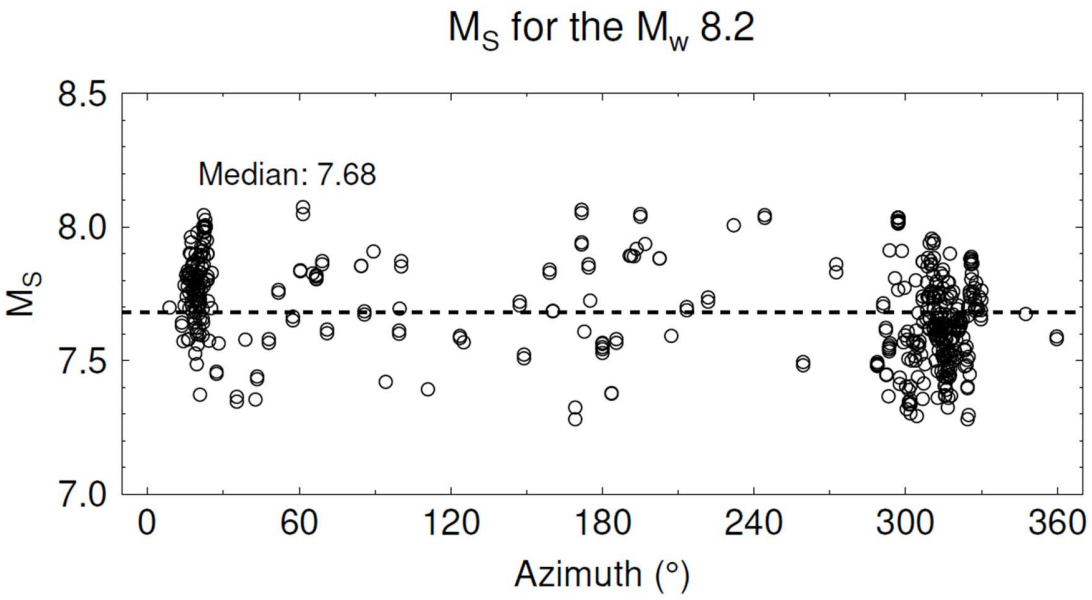

Figure S5. Surface wave magnitudes of the South Sandwich Island sequence. (a) Individual surface wave magnitudes M_S using stations at different azimuths (black circles) for the overall M_w 8.2 South Sandwich Island sequence. The black dashed line shows the median m_S of 7.68.

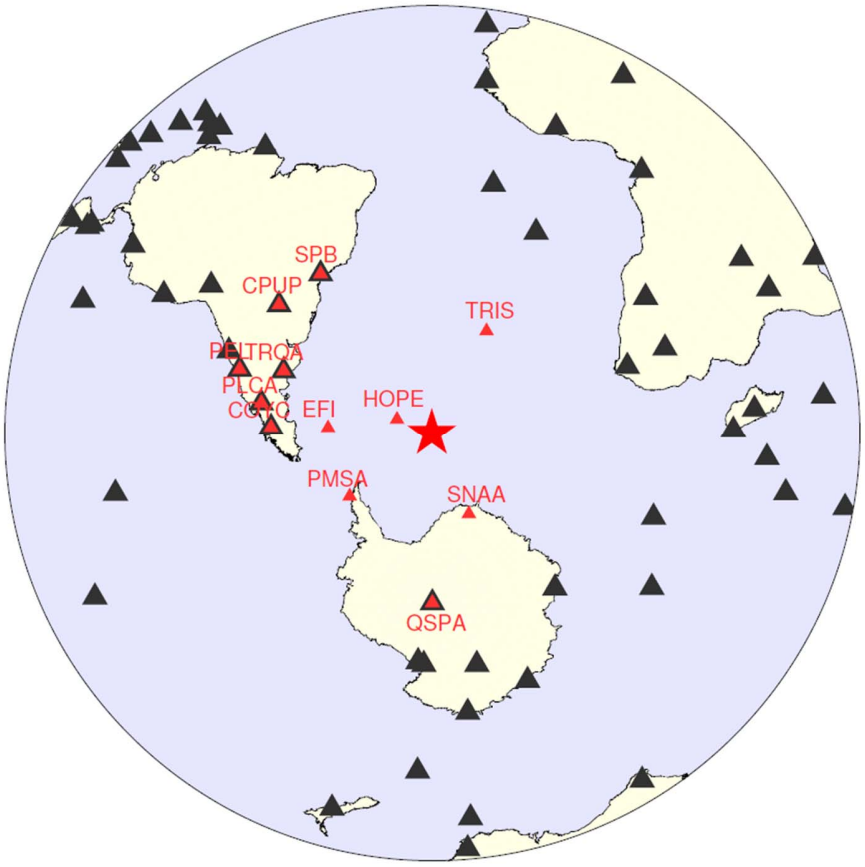

Figure S6. Seismic stations used in the subevent inversion. The red star shows the hypocenter of the South Sandwich Island sequence. Black and red triangles indicate the teleseismic (epicentral distance between 30° and 90°) and regional (epicentral distance within 40°) stations. Note that 7 of them are used for both teleseismic and regional inversions.

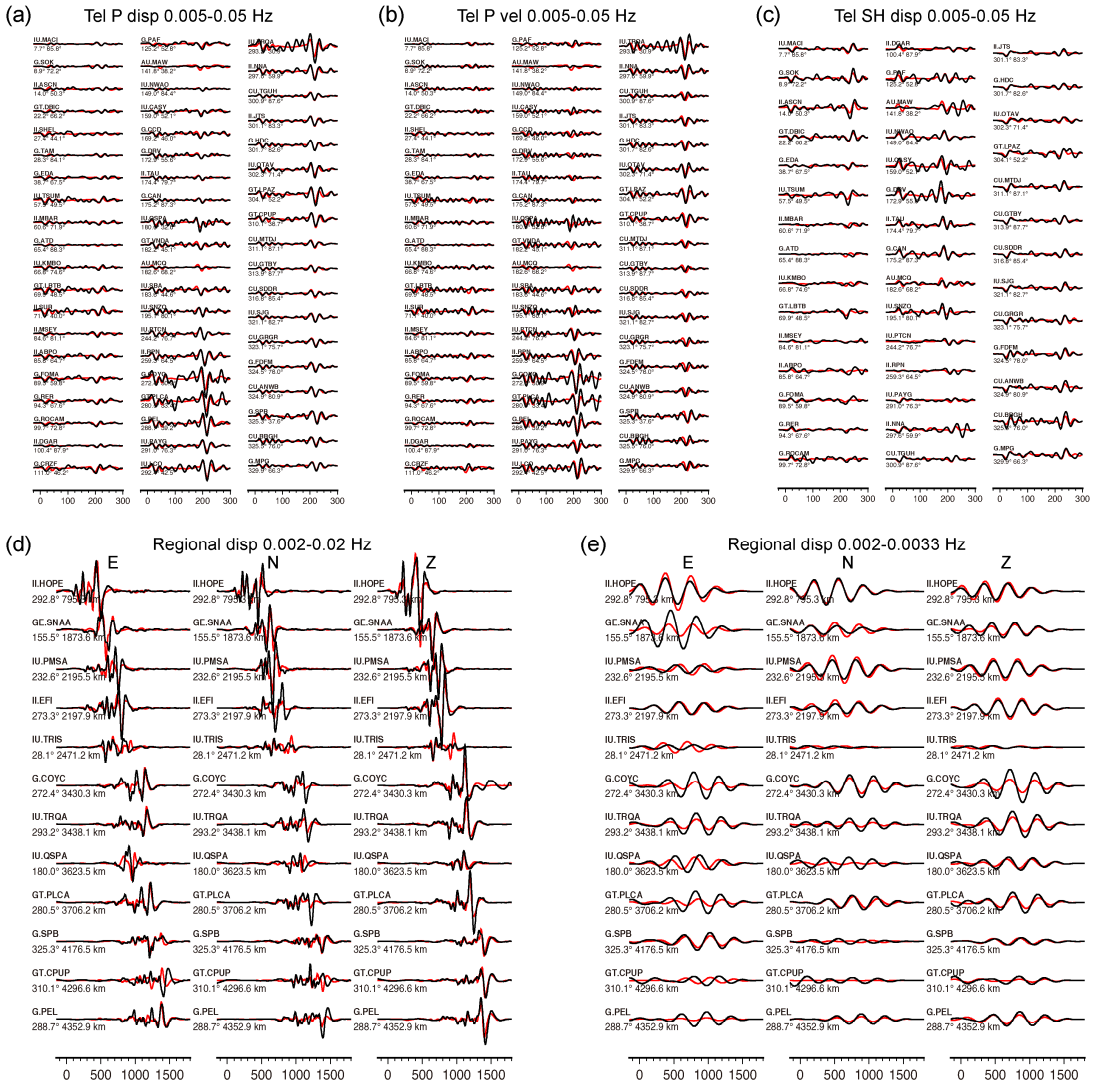

Figure S7. Waveform fits of the preferred subevent model for the South Sandwich Island sequence. Observed data and synthetics are indicated by black and red lines, respectively. The numbers leading each trace are the station azimuth and distance. (a) P waves in displacement. (b) P waves in velocity. (c) SH waves in displacement. (d) Intermediate period (0.002-0.02 Hz) regional full waveforms in displacement. (e) Long period (0.002-0.0033 Hz) regional full waveforms in displacement.

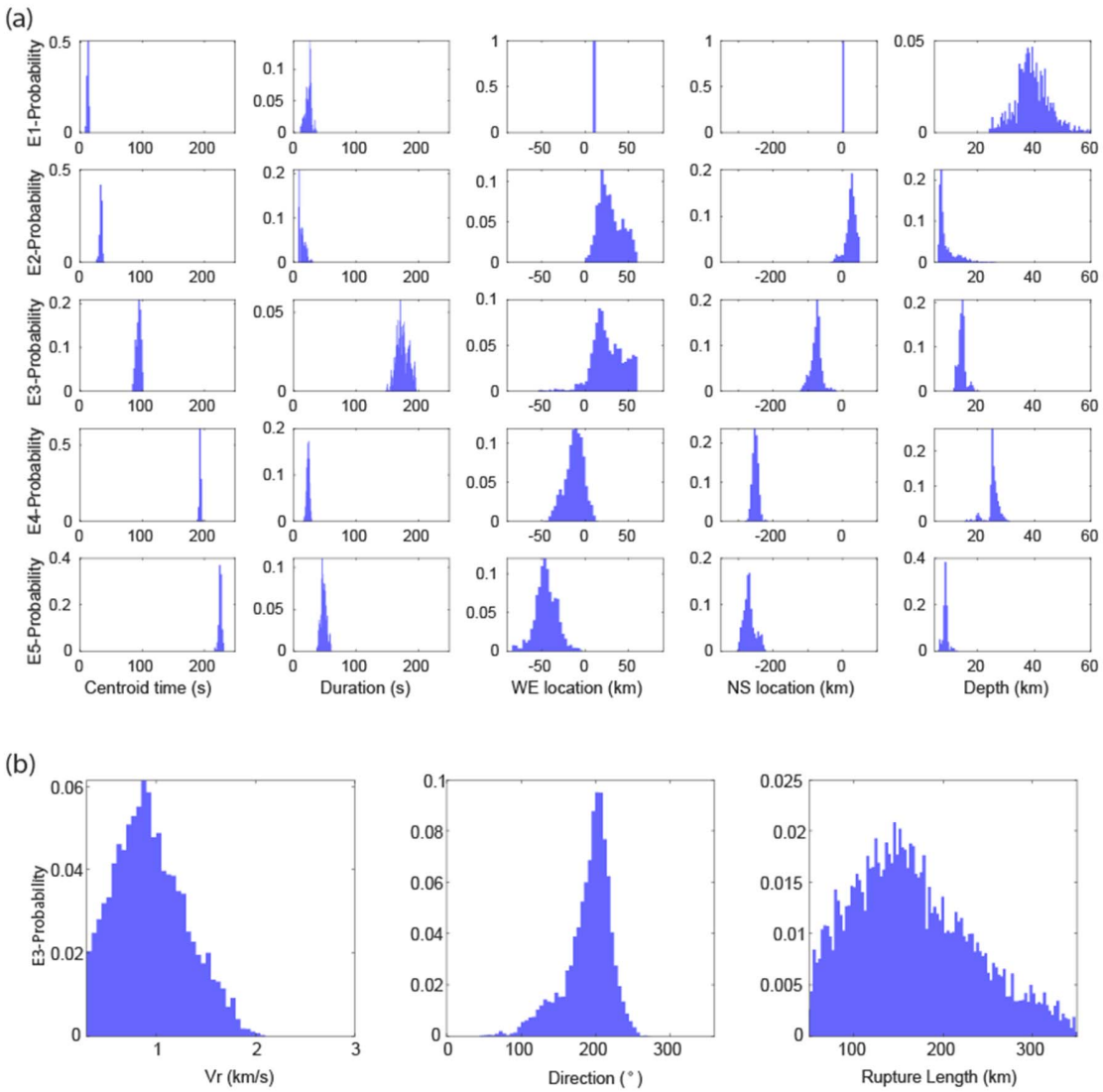

Figure S8. Assessment of subevent model uncertainties with the Markov Chain sample distributions. (a) Markov Chain sample distributions of the point source parameters. Columns from left to right indicate the density distribution of subevent centroid times, durations, west-east locations, north-south locations and centroid depths. Rows represent subevents E1-E5. (b) Markov Chain sample distributions of finiteness parameters for the subevent E3. Columns are the rupture velocity, rupture direction (in degrees clockwise from the north), and rupture length.

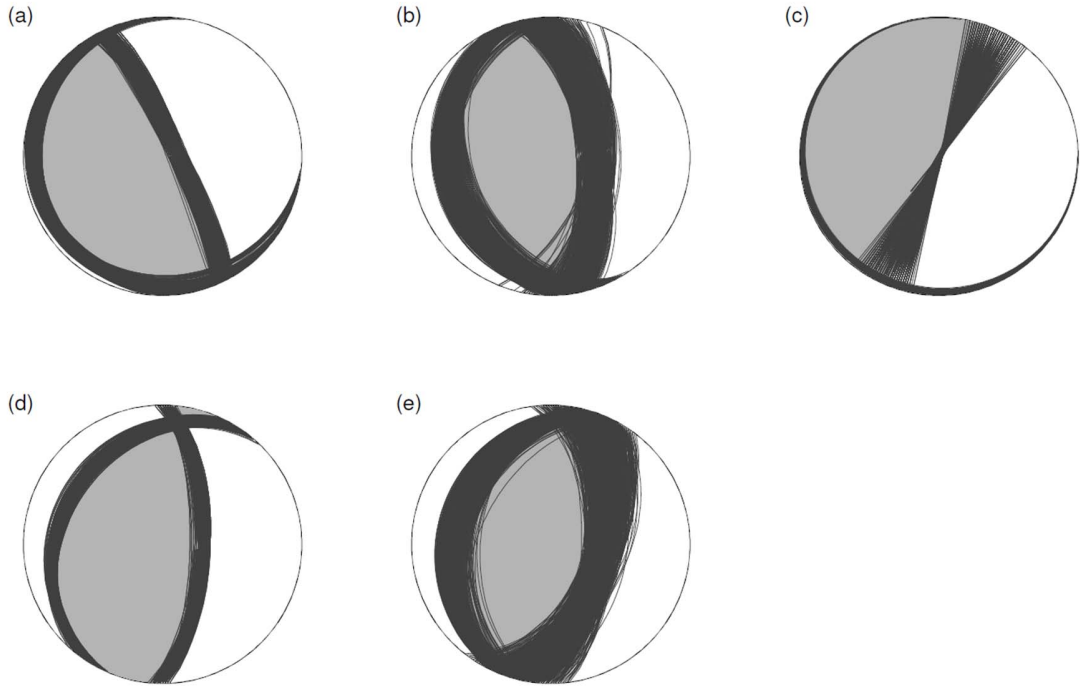

Figure S9. Ranges of double couple focal mechanisms for subevent E1 (a), E2 (b), E3 (c), E4 (d) and E5 (e) of the South Sandwich Island sequence.

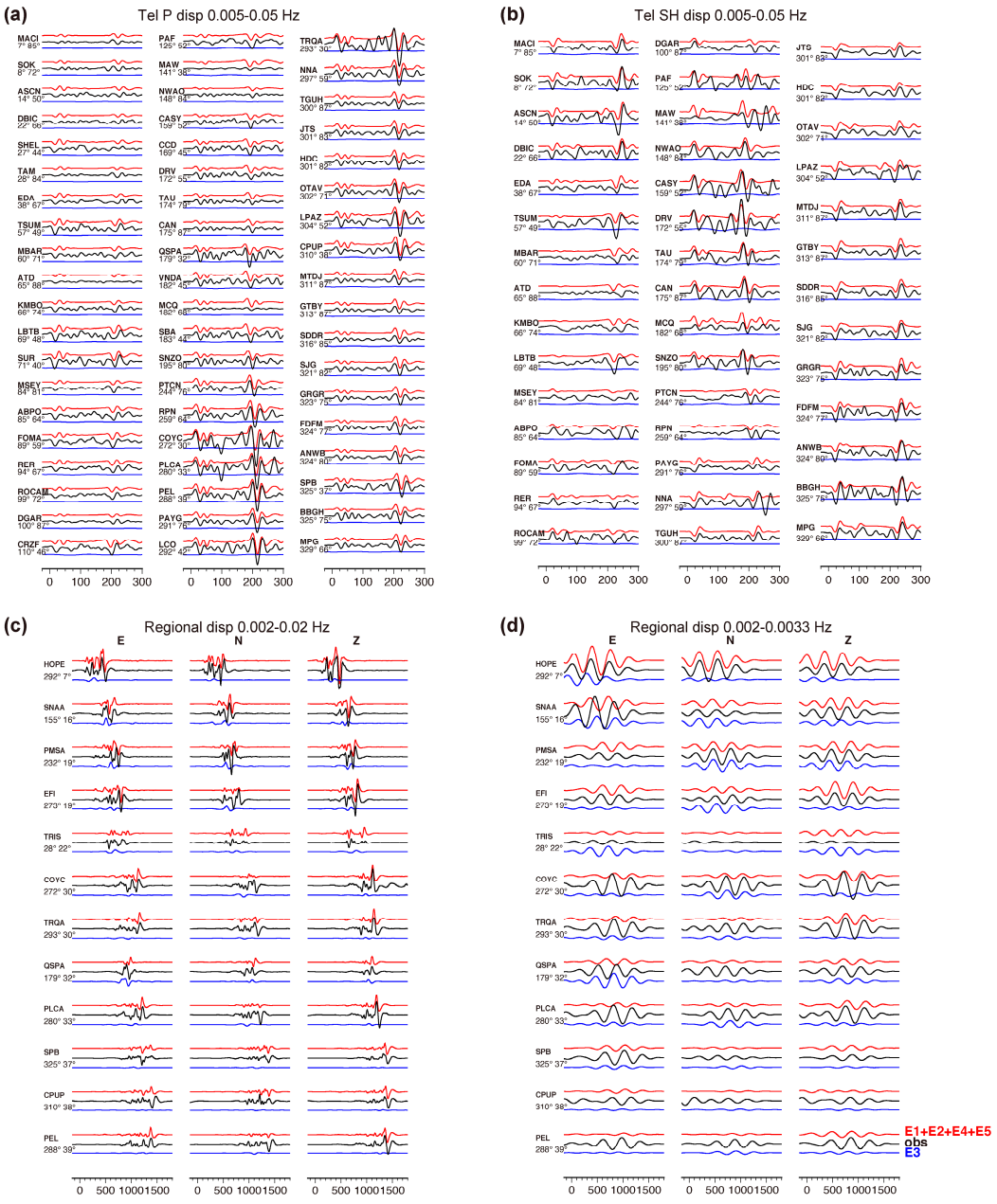

Figure S10. Contributions to waveforms from different groups of subevents. Black lines show the observed seismograms. Red lines represent the total contributions from regular subevents E1, E2, E4 and E5. Blue lines indicate the contribution from the slow subevent E3. Numbers leading traces are the station azimuths and distances. (a) P waves in displacement. (b) SH waves in displacement. (c) Intermediate period (0.002-0.02 Hz) regional full waveforms in displacement. (d) Long period (0.002-0.0033 Hz) regional full waveforms in displacement.

	Initiation time (UTC)	Centroid time (UTC)	Longitude (°)	Latitude (°)	Depth (km)	Magnitude	Strike (°)	Dip (°)	Rake (°)
NEIC1	18:32:52	NaN	-25.03	-57.68	47.2	7.5	NaN	NaN	NaN
NEIC2	18:35:17	NaN	-25.26	-58.38	22.8	8.1	NaN	NaN	NaN
GCMT1	NaN	18:35:25	-24.34	-59.48	20.0	8.3	204	14	118
GCMT2	NaN	18:36:13	-25.15	-60.47	15.1	7.9	195	22	64
USGSMwc	NaN	18:35:58	-24.90	-60.38	10.0	7.98	248	27	151
USGSMww	NaN	18:36:56	-23.16	-60.80	35.5	8.13	223	11	110
W-phase	NaN	18:35:33	-26.88	-60.22	30.5	8.12	222	14	112

Table 1. Source parameters for the South Sandwich Island earthquake from different catalogs.

	Centroid time (s)	Duration (s)	Longitude (°)	Latitude (°)	Rupture Velocity (km/s)	Rupture direction (°)	Depth (km)	Mrr (10^{20} N-m)	Mtt (10^{20} N-m)	Mpp (10^{20} N-m)	Mrt (10^{20} N-m)	Mrp (10^{20} N-m)	Mtp (10^{20} N-m)
E1	13.08	22.74	-25.03	-57.57	NaN	NaN	39.38	0.314	-0.104	-0.211	-0.301	0.669	0.083
E2	35.72	19.37	-24.82	-57.34	NaN	NaN	7.09	0.747	-0.151	-0.595	0.018	0.551	0.095
E3	90.38	176.12	-24.72	-58.28	1.01	187.06	14.26	2.469	-1.547	-0.922	8.191	19.743	2.049
E4	195.01	26.33	-25.64	-59.86	NaN	NaN	25.28	2.153	-0.304	-1.849	-0.236	2.268	-0.622
E5	226.37	50.40	-25.86	-60.00	NaN	NaN	8.94	3.315	-0.940	-2.375	0.704	2.917	-0.512

	Mo (10^{20} N-m)	M_w	Strike (°)	Dip (°)	Rake (°)
E1	0.79	7.20	150	11	84
E2	0.88	7.23	164	26	79
E3	21.58	8.16	134	4	22
E4	3.11	7.59	213	24	118
E5	4.25	7.69	199	22	94

Table 2. Subevent model parameters for the South Sandwich Island earthquake.